

# Next-Generation 5/10 kW Ion Propulsion Development Status <sup>\*†</sup>

Michael J. Patterson, John E. Foster, Thomas Haag, Luis Pinero,  
Vincent K. Rawlin, George C. Soulas, and Michelle S. Doehne  
National Aeronautics and Space Administration

Glenn Research Center

MS 301-3

21000 Brookpark Road

Cleveland, Ohio 44135

216-977-7481

[Michael.J.Patterson@grc.nasa.gov](mailto:Michael.J.Patterson@grc.nasa.gov)

Robert F. Roman

QSS Group, Inc.

Cleveland, Ohio

IEPC-01-089

**The NASA Glenn Research Center ion propulsion program addresses the need for high specific impulse systems and technology across a broad range of mission applications and power levels. One activity is the development of the next-generation ion propulsion system as follow-on to the successful Deep-Space 1 system. The system is envisioned to incorporate a lightweight ion engine capable of operating over 1-10 kW, with a 550 kg propellant throughput capacity. The engine concept under development has a 40 cm beam diameter, twice the effective area of the Deep-Space 1 engine. It incorporates mechanical features and operating conditions to maximize the design heritage established by the Deep-Space 1 engine, while incorporating new technology where warranted to extend the power and throughput capability. Prototype versions of the engine have been fabricated and are under test, with an engineering model version in manufacturing. Preliminary performance data for the prototype engine has been documented over 1.1-7.3 kW input power. At 7.3 kW, the engine efficiency is 0.68, at 3615 seconds specific impulse. Critical component temperatures including the discharge cathode assembly and magnets have been documented and are within established limits, with significant margin relative to the Deep-Space 1 engine.**

## Introduction

With the success of the NASA Solar Electric Propulsion Technology Applications Readiness (NSTAR) program ion propulsion system on the Deep-Space 1 spacecraft,<sup>1</sup>

the future for this propulsion technology for other NASA missions, and missions of national interest, appears promising. The 2.5 kW ion propulsion system on Deep-Space 1 has performed flawlessly in space, operating over 13,000 hours and processing in excess of 60 kg of

<sup>\*</sup>Presented as Paper IEPC-01-089 at the 27<sup>th</sup> International Electric Propulsion Conference, Pasadena, CA, 15-19 October, 2001.

<sup>†</sup>This paper is declared a work of the U.S. Government and is not subject to copyright protection in the United States.

xenon propellant.

The successful demonstration of the NSTAR ion thruster has provided future mission planners with an off-the-shelf 2.5 kW ion thruster. While the NSTAR thruster is appropriate in terms of power level and lifetime for Discovery Class as well as other, smaller NASA missions, its application to large flag-ship type missions such as outer planet explorers and sample return missions is limited due its lack of power and total impulse capability.

Several missions under consideration for the Exploration of the Solar System, part of NASA's Space Science Enterprise, have identified a higher power, higher throughput capability, 5/10-kW ion propulsion system as an enabling technology. These missions include the Europa Lander, the Saturn Ring Observer, the Neptune Orbiter, and the Venus Surface Sample Return.<sup>2,3</sup>

At the 15-25 kW power levels and long burn times proposed for these missions the required number of NSTAR thrusters would prove expensive, complex, large, and heavy to integrate with a spacecraft. Studies for comet and Mars sample return missions as well as outer planet orbiters such as Titan explorer and Neptune orbiter have all shown the need for a higher power, higher total impulse capability thruster to minimize the propulsion system size, mass and complexity. As such a next generation 5/10-kW ion thruster based on the design successes learned from the NSTAR program is being developed.

NASA Glenn Research Center (GRC) is pursuing ion technology development for a range of mission applications, including the aforementioned opportunities. This includes the development of the next-generation ion propulsion system, envisioned as a high performance, low cost system capable of operating at 10 kW per engine. Specific goals for this next-generation ion propulsion system include:

1. 1.0-10 kW engine power throttling range appropriate for both Earth-orbit applications of national interest, and primary propulsion for deep-space interplanetary missions (4x increase in input power and 2.5x increase in throttling range over the NSTAR propulsion system);

2. 550 kg engine throughput capability delivering a total impulse of  $2.1 \times 10^7$  N-s (6x increase over the NSTAR thruster);
3. 12 kg thruster mass with mechanical design envelope comparable to the NSTAR thruster, and a 92% efficient, 27 kg power processor mass (3x and 2x reduction in specific mass for the thruster and power processor respectively compared to NSTAR); and
4. a flight system cost target of 1/2-NSTAR recurring cost.

This paper discusses the on-going activities to develop the next-generation ion propulsion system.

### Technical Approach

The approach used in the development of the engine was to first conduct detailed performance and lifetime projections which would yield design requirements; discharge electrical efficiency, neutralizer propellant consumption, ion optics electrode geometry, and low-wear rate, temperature tolerant components. One output of the design analyses was selection of the appropriate engine beam diameter. The design analyses included results obtained from numerous tests of a 30 cm NSTAR engineering model (EM) thruster which was power-throttled to greater than 5 kW to quantify critical component temperatures, operating voltages, and beam current density profiles.

A 'derating' approach, similar to that implemented in the NSTAR program, was implemented to best preserve the NSTAR design heritage. This is a design approach that reduces operating voltages, and maintains low beam current densities and component operating temperatures; an approach most likely yielding the desired performance goals. From this activity, an NSTAR-derivative engine with 40 cm beam diameter was selected. An engine of this size has twice the beam area of the NSTAR 30 cm (28 cm beam diameter) thruster. Increasing the engine beam diameter from 28 cm to 40 cm doubles the area which provides higher power capability while maintaining comparable operating voltages and current densities, as well as design and manufacturing processes for components, etc..

At an input power of 4.7 kW, the engine would be operating at approximately the same operating voltages and beam current density as the 2.3 kW NSTAR thruster, and hence would be expected to yield the same operating life time, but producing twice the thrust. At 10 kW input power, the 40 cm engine would be operating at about 1.6x the current density of the NSTAR thruster. With the flight spare NSTAR thruster having demonstrated more than 150 kg propellant throughput capability in ground-testing<sup>4</sup> (substantially higher than the 83 kg original design goal) a 2x increase in throughput capability for the 40 cm thruster would be anticipated. With the implementation of advanced ion optics designs including thick-accelerator molybdenum electrode designs, and titanium electrodes, the capability of the engine should be pushed beyond the 550 kg goal.

Two prototype (laboratory) versions of the 40 cm engine have been designed, developed, manufactured and assembled in-house at GRC for performance testing, now underway. Engineering model (EM) engine designs, based on both prototype concepts, have been completed and manufacturing and assembly of this hardware is ongoing. The design of several of the components for the EM engines, including the spun-formed discharge chamber, hollow-cathodes, and ion optical system, are derived from the NSTAR engine technology. Testing of the EM engines is to begin prior to the end of the calendar year.

In addition to the engine development effort in-house, a contracted activity for the development of a breadboard power processor was initiated with Boeing Electron Dynamic Devices. The beam power supply has been fabricated and delivered, with completion of the full power processor to occur in the second phase of the contract.<sup>5</sup> A contracted activity to manufacture an advanced-EM engine based on the NASA-developed design is also anticipated.

## Thruster

### Performance Goals

This section discusses the performance goals for the 40 cm engine.

### Assumptions

The 40 cm diameter ion optics are expected to have a perveance per unit area comparable to that of the optics developed by NASA GRC for the Deep Space One (DS1) engine. A 0.66 mm grid-gap, and 2800 V/mm maximum electric field strength was assumed which is well within demonstrated capabilities. The minimum total voltage, in volts, is then given by:

$$V_{t-\min} = (I_b / (9.06 \cdot 1 \times 10^{-5}))^{0.67} \quad [1]$$

where  $I_b$  is the beam current in amperes. An operating margin of 250 V is added to the  $V_{t-\min}$  calculated from equation 1 to define the beam power supply voltage, assumed to be at a net-to-total voltage of 0.82.

The magnitude of the accelerator grid voltage, in volts, is estimated from:

$$V_{\text{accel}} = (B \cdot I_b) / (A_b \cdot F_b) + C \quad [2]$$

where  $B$  is a constant equal to 10 V-cm<sup>2</sup>/ma,  $A_b$  is the beam area in cm<sup>2</sup>,  $F_b$  is the beam flatness parameter (estimated to be 0.60), and  $C$  is a constant equal to 181 V. Equation 2 is derived from an empirical equation used to determine the electron backstreaming limit,<sup>6</sup> with 50 V margin added. The accelerator grid drain current is estimated to be 0.34% of the beam current, based on acceptance data for the DS1 ion optics.<sup>7</sup>

The projected discharge losses for the 40 cm engine are derived from the dependency of DS1 thruster discharge losses with beam current at fixed discharge propellant efficiency. These are then adjusted to accommodate the improved performance associated with the larger volume-to-surface area of the 40 cm engine chamber. The engine is expected to operate at about a 0.90 discharge propellant efficiency. The discharge losses for the 40 cm, in W/A, at a 0.90 discharge propellant efficiency, are estimated to be:

$$e_i = A + 108 \cdot e^{-(I_b - 0.5) / 0.454} \quad [3]$$

where  $I_b$  is the beam current and  $A$  is given by:

$$\left. \begin{array}{l} A = 250 \text{ W/A for } 0.88 < I_b < 1.20 \text{ A} \\ A = 190 \text{ W/A for } I_b = 1.20 \text{ A} \\ A = 150 \text{ W/A for } I_b > 1.20 \text{ A} \end{array} \right\} [4]$$

A discharge voltage of 24 volts is assumed for the throttling range of the 40 cm diameter engine. This is the nominal operating voltage for the DS1 thruster discharge, and it is approximately equal to the estimated threshold energy for sputtering of molybdenum, assumed to be four times the heat of sublimation.<sup>8</sup> Using a discharge voltage of 24 volts for the entire power throttling range and the discharge losses estimated from Equation 1, the cathode emission current requirement for the 40 cm engine can then be calculated directly from:

$$I_e = e_i \cdot I_b / V_d \quad [5]$$

where  $V_d$  is the discharge voltage in volts. The cathode emission current may be approximated by:

$$I_e = 7.92 + 2.90 \cdot P_{in} \quad [6]$$

where  $P_{in}$  is the engine input power in kilowatts. At 1 kW, the cathode emission current requirement is estimated to be approximately 10.8 A, and at 10 kW it is approximately 37 A.

The neutralizer is assumed to have keeper and coupling voltages of 18 and -17 volts respectively, at a fixed keeper current of 1.0 A. It must operate at higher emission currents (beam plus keeper currents) than the DS1 neutralizer; from about 2.2 A at 1.0 kW to about 6.8 A at 10 kW. This yields a modest 3.1:1 ratio in maximum-to-minimum emission current requirement. The neutralizer propellant flow rate dependency on beam current is expected to be (in mg/sec):

$$\dot{m}_n = 0.070 + 0.102 \cdot I_b \quad [7]$$

Equation 7 is based on the performance of a lower-power neutralizer developed as a replacement for the DS1 neutralizer.<sup>9</sup>

The overall engine performance parameters can then be estimated based on the quoted assumptions. The engine thrust can be determined from:

$$F = g \cdot \left(2 \frac{m}{q}\right)^{1/2} \cdot I_b \cdot (V_b)^{1/2} \quad [8]$$

where  $g$  is a total thrust-loss correction factor,  $m$  is the ion mass,  $q$  is the ion charge, and  $V_b$  is the beam voltage. The total thrust-loss correction factor,  $g$  includes a factor for doubly-charged ions, and for off-axis beamlet vectoring.<sup>10</sup>

The beam voltage,  $V_b$ , is equivalent to the beam power

supply voltage minus the absolute value of the neutralizer coupling voltage.

The specific impulse can be calculated from:

$$I_{sp} = h_u \cdot g \cdot \left(2q \frac{V_b}{m}\right)^{1/2} \cdot \frac{1}{g} \quad [9]$$

where  $h_u$  is the propellant efficiency, which is the ratio of the beam current to the total propellant flow rate, and  $g$  is acceleration due to gravity. The total propellant flow rate,  $\dot{m}_T$ , includes the xenon flow into the discharge cathode and main plenum, and neutralizer, plus an additional term to account for propellant flow ingested from the facility back into the discharge chamber through the ion optics.<sup>10</sup>

The input power can be calculated from:

$$P_{in} = (V_{bps} \cdot I_{bps}) + (V_{anode} \cdot I_{anode}) + (|V_{accel}| \cdot I_{accel}) + (V_{nk} \cdot I_{nk}) \quad [10]$$

where  $V_{bps}$  and  $I_{bps}$  are the voltage and current of the beam power supply,  $V_{anode}$  and  $I_{anode}$  are the voltage and current of the discharge power supply,  $V_{accel}$  and  $I_{accel}$  are the voltage and current of the accelerator power supply, and  $V_{nk}$  and  $I_{nk}$  are the voltage and current of the neutralizer keeper power supply.

The total engine efficiency is then given by:

$$h = \frac{F \cdot I_{sp} \cdot g}{2 \cdot P_{in}} \quad [11]$$

#### Nominal Operation

Overall performance numbers were calculated for the 40 cm engine, over a range of beam currents from 1.20 A to 5.80 A (corresponding to propellant flow rates from 2.05 mg/sec to 9.43 mg/sec), and these are shown in Table I. At 1.20 A, the average beam current density is 34% of that of the DS1 engine operating at full power (1.76 A beam current, or 2.92 ma/cm<sup>2</sup>). At 5.80 A (10 kW operation), the average beam current density is 164% of the DS1 engine at full power. At 5 kW operation, or about 3.52 A beam current, the average beam current density is the same as the DS1 engine at 2.3 kW.

At each beam current, the engine performance was calculated at the required total voltage, and then throttled down in power by decreasing the beam current at fixed

total and beam power supply voltages. Performance projections for the engine are given in Table I, and in Figures 1-3.

In Fig. 1, the maximum range of thrust and input power are given for a number of values of specific impulse, from 3900 seconds to 2500 seconds. Of note is that the maximum thrust and power throttling ranges occur at the highest specific impulse, and diminish with decreasing specific impulse. At 3900 seconds, the thrust and power range from approximately 76-360 mN, and 2.1-10 kW, respectively. At 3100 seconds, the thrust and power ranges are 61-137 mN and 1.5-3.2 kW respectively. Figure 2 is a plot of the maximum thrust versus input power, taken from the data of Figure 1. The thrust ranges from approximately 49 mN at 1.1 kW to approximately 360 mN at 10 kW. The flow rate at full power is nearly 10 mg/s. Figure 3 shows the corresponding values of (maximum) engine efficiency and specific impulse; 56% at about 2500 seconds, to 72% at about 3900 seconds.

Table I - Nominal

$\dot{m}_T$ , mg/sec	F, mN	$I_{sp}$ , sec	$P_{in}$ , kW	Eff.
1570 V $V_{bps}$				
9.43	364	3945	10.0	0.72
7.81	299	3900	8.20	0.71
5.82	221	3885	6.08	0.71
4.49	170	3865	4.67	0.70
2.05	75.6	3760	2.16	0.66
1400 V $V_{bps}$				
7.81	282	3680	7.39	0.70
5.82	209	3665	5.48	0.70
4.49	160	3645	4.21	0.69
2.05	71.3	3565	1.96	0.65
1180 V $V_{bps}$				
5.82	192	3365	4.71	0.68
4.49	147	3345	3.62	0.68
2.05	65.4	3255	1.69	0.63
1020 V $V_{bps}$				
4.49	137	3110	3.19	0.67
2.05	60.8	3025	1.50	0.61
680 V $V_{bps}$				
2.05	49.4	2460	1.09	0.56

#### High-Thrust Density Operation

Performance projections were made for the 40 cm at high thrust density using the same assumptions listed previously, with the exception of a variable net-to-total voltage (R-ratio) and a perveance margin of 150 V. These values are shown in Table II. For these estimates, an R-ratio between 0.2 and 0.9 was assumed.<sup>10</sup> Power throttling the engine is achieved by maintaining a fixed maximum beam current of 5.80 A and varying the R-ratio. This yields higher thrust and lower specific impulse at throttled conditions. At 3.2 kW input power a 26% increase in thrust is achieved. However it does so at increased accelerator grid voltage that exacerbates charge-exchange erosion. For operation at the high-thrust density conditions identified in Table II, carbon-based ion optics will be required to yield useful engine life.

Table II – High-Thrust Density

$V_{bps}$ , V	F, mN	$I_{sp}$ , sec	$P_{in}$ , kW	Eff.
$\dot{m}_T = 9.43$ mg/sec				
1575	366	3970	10.1	0.71
1120	305	3340	7.44	0.67
670	232	2570	4.81	0.60
400	173	1960	3.23	0.50

#### High Specific Impulse Operation

Performance projections for the 40 cm engine operating at increased specific impulse were calculated, and are given in Table III. Power throttling was achieved by varying the beam current from 5.80 A down to 0.88 A at fixed beam power supply voltage and fixed total voltage. For these estimates, the ion optics interelectrode (grid) gap was assumed to be 1.24 mm, with a 2500 V/mm maximum electric field strength. The minimum total voltage (estimated from Equation 1) was increased by multiplying by a factor to account for the larger grid gap, and then a 150 V margin was added. The factor for increased grid gap was equal to 1.46, estimated from:

$$F_{V-\min} = (\ell_{\text{High-Isip}} / \ell_{\text{Nominal}})^{4/3} \quad [12]$$

where  $\ell_{\text{High-Isip}}$  and  $\ell_{\text{Nominal}}$  are the effective acceleration lengths for the optics for the high specific impulse operation, and the nominal operation, respectively. The effective acceleration length is given by:<sup>10</sup>

$$\ell = [(\ell_g + t_s)^2 + (d_s / 2)^2]^{0.5} \quad [13]$$

where  $\ell_g$  is the grid gap,  $t_s$  is the screen electrode thickness, and  $d_s$  is the screen electrode hole diameter.

As indicated in Table III, the specific impulse varied from about 4700 seconds at 2.5 kW to about 5000 seconds at 13 kW. The reduction in specific impulse with reduction in power is due to the increasing fraction of propellant going through the neutralizer, and the assumption of a fixed output voltage from the beam power supply. A comparison of the estimated engine efficiencies versus specific impulse for nominal, high-thrust density, and high specific impulse operation is shown in Figure 4.

Table III – High-Specific Impulse

$\dot{m}_T$ , mg/sec	F, mN	$I_{sp}$ , sec	$P_{in}$ , kW	Eff.
2540 V $V_{bps}$				
7.81	381	4980	12.8	0.73
5.82	283	4955	9.52	0.72
4.49	217	4930	7.31	0.72
2.05	96	4800	3.33	0.68
1.53	71	4715	2.52	0.65

### Mechanical Design

Figure 5 shows an outline of the external dimensions of one of the two 40 cm beam diameter engine designs under development superimposed on the 30 cm beam diameter NSTAR DS1 flight thruster. As shown, while the beam area of the new engine is twice that of the DS1 thruster, the mechanical envelope (maximum width and length) is not substantially larger than the DS1 thruster. The overall dimensions of the 40cm beam diameter engine are 52 cm diameter by 33 cm length. The engine configuration depicted in Fig. 5 is referred to as a partial-conic geometry, based on its discharge chamber design. A second engine configuration, using a full-conic discharge chamber, has identical maximum exterior dimensions. The goal for the engine mass is 12 kilograms.

### Discharge Chamber

Two different chamber geometry designs are under investigation for the 40 cm engine; a partial-conic, and full-conic geometry. Prototype and engineering model versions of both discharge chambers have been manufactured. Mild steel is used in the construction of the discharge chambers. The prototype chambers were rolled and welded from sheet metal, while the

engineering model hardware was spun-formed. Figure 6 shows the discharge chambers for the EM engines under assembly.

The 40 cm engine uses a ring-cusp magnetic circuit, with high-field strength permanent magnets for plasma containment.<sup>11</sup> The magnets form rings of alternating polarity along the rear and sides of the anode-potential discharge chamber walls. Final magnetic circuit configurations were established after a series of engine tests with beam extraction were completed, aided by the use of a magnetic field code.

A flake-retention scheme (to ensure adherence of sputtered coatings to chamber wall surfaces) is employed in the discharge chamber, which also functions as a magnet mechanical retainer. The material, preparation, and installation processes employed for the flake-retention system are identical to those implemented on the DS1 thruster. The 40 cm engine also incorporates a reverse-feed propellant injection process for the main plenum to increase discharge propellant utilization efficiency at throttled conditions.

### Cathodes

Several prototype cathode assemblies for the 40 cm engine have been fabricated and either integrated with the engine, or characterized separately in bell-jar testing. The discharge cathode assembly incorporates a 12.7 mm diameter cathode tube, has an enclosed-keeper electrode, and uses similar design and manufacturing processes as those employed in the DS1 thruster discharge cathode. A photo of one such assembly is shown in Figure 7. The cathode employs an emitter substantially larger than that used in the DS1 thruster cathode, which should yield longer operating life at equivalent operating temperatures.

The neutralizer cathode under development for the 40 cm engine is similar in mechanical design to that used on the DS1 thruster. It has an enclosed-keeper geometry, and by external perspective is identical in geometry to that used on the DS1 thruster. However, critical internal dimensions for the emitter, and cathode and keeper orifice plates are adjusted to accommodate the higher emission current requirements for the 40 cm engine, and do so at reduced ratios of propellant flow rate-to-emission current.

### *Ion Optics*

Two design approaches are being pursued for the 40 cm ion optics. These include NSTAR-type electrodes of increased beam diameter, and an alternate geometry. The alternate geometry is a two-grid design constructed of molybdenum with an accelerator electrode with thickness 1.5x that of NSTAR, to increase life. The electrode mounting system is scaled from the NSTAR design and also uses the same materials as that implemented in the 30 cm thruster. The 40 cm optics use the same aperture geometry as that of the NSTAR optics to take advantage of the large database of lifetime and performance data available.

Dome-shaped grids are used for the 40 cm ion optics because they are well suited for large-area optics designs. A dome height-to-chord radius ratio similar to that of the NSTAR grids is used because it addresses issues associated with grid fabrication and thruster operation and because it is acceptable from thermal expansion and launch stress standpoint.

To date 40 cm diameter electrodes has been fabricated (see Fig. 8, NSTAR-type electrodes). No issues were encountered during manufacturing. Additional sets are presently in fabrication, including sets with increased accelerator electrode thickness.

### **Performance Data**

Preliminary performance data for the first of two prototype 40 cm engine designs are documented below (the partial-conic discharge chamber design), and it includes engine throttling over the ‘nominal operating’ conditions up to about 7.3 kW discussed earlier. The engine tests used 50 cm diameter ion optics (which were masked down by the smaller discharge chamber diameter) because the 40 cm diameter optics were in fabrication at the time of this publication.

All engine testing was performed at NASA GRC, in Vacuum Facility 11 (VF11). VF11 is 2.2-m in diameter by 9.0-m in length with four ports isolated with pneumatic gate valves. Four 0.9-m diameter and three 1.2-m diameter helium cryopumps yield a pumping speed of approximately 240,000 liters per second (nitrogen). Two of the four facility ports each have integral 0.25-m helium cryopumps with a pumping speed of 4000 liters

per second (nitrogen). This allows the ports to be operated either as facility ports or stand-alone bell jars. A 2-D motion control system drives a rake of electrostatic probes through the plasma plume, and resident optical diagnostics include CCD cameras and a 0.5-m spectrometer for observation and spectroscopy.

Cathode temperature characterization tests were performed in a small cryopumped bell jar at NASA GRC (VF62). VF62 is a 0.33-m diameter by 0.8-m long stainless steel bell jar, evacuated with a 0.25-m helium cryopump with a pumping speed of 4,000 liters per second (nitrogen). With automated data acquisition and control systems, power consoles, and integral high-purity propellant feed systems, VF62 is used for conducting component-level performance and life tests. Cathode temperature data were taken using a planar anode without a magnetic circuit.

### *Discharge Chamber*

Some design and test iterations were initially required to optimize the discharge magnetic circuit design. The discharge losses for the prototype 40 cm engine are shown in Figure 9, plotted against extracted beam current. The data in Figure 9 are for discharge propellant efficiencies of  $0.90 \pm 0.01$ . Also shown is the predicted performance, from equations 3 and 4 (identified as ‘goal’).

As indicated, the demonstrated discharge losses compare favorably to the predicted values at the lowest beam current of 1.2 Amperes. Losses varied from about 220-232 W/A, depending upon the ion optics voltages, compared to about 273 W/A predicted. At the maximum beam current of about 4.72 A, the engine losses were about 147 W/A, which also compare favorably to the predicted value of 150 W/A. However at intermediate beam currents, the engine losses were somewhat higher than predicted. The engine losses, in W/A, for this discharge configuration can be estimated from:

$$e_i = 7.30 \cdot (I_b)^2 - 66.1 \cdot I_b + 296 \quad [14]$$

At 1.76 A beam current, the discharge losses for this discharge are approximately the same as the DS1 engine discharge. Additional magnetic circuit modifications are anticipated to reduce losses further.

Figure 10 is a plot of discharge losses versus discharge propellant efficiency for two different beam currents. At 1.20 A, corresponding to the 2.1 mg/sec operating conditions of Table I, the discharge operated at about 198 W/A at 0.85 propellant efficiency and 26 V discharge voltage. At this beam current, a discharge voltage of 28 V was required to yield propellant efficiencies of 0.90. For beam currents of  $\geq 2.70$  A, corresponding to propellant flow rates of  $\geq 4.55$  mg/sec from Table I, 0.90 propellant efficiencies were achievable at 24 volts discharge, as indicated in Figure 10.

During 40 cm engine testing, the discharge chamber was instrumented with thermocouples to quantify magnet temperature as a function of input power. Figure 11 shows the magnet temperature as a function of discharge power. The temperatures correspond to the most-down stream ring of magnets in the discharge chamber near the ion optics, which were slightly higher than in other locations of the discharge. As indicated, the magnet temperatures varied from about 175 deg C at 240 W, to about 260 deg C at 700 W. This range of temperatures and discharge power levels correspond to 1.5 kW to 7.3 kW engine input power. From the trend line of Figure 11, the maximum magnet temperatures at 10 kW (about 860 W discharge power) are expected to be about 275 deg C.

For the DS1 thruster, the maximum magnet temperatures during full power operation (2.3 kW) were approximately 310 degrees centigrade, or about 40 degrees below their operating limit. The data of Figure 11 for the 40 cm engine indicate considerable thermal margin.

#### *Discharge Cathode*

Discharge cathode conditioning and ignition were conducted using protocols developed for the DS1 and Space Station cathodes. Ignition of the discharge cathode occurred within 6 minutes of energizing the swaged heater to a pre-defined input current.

Figure 12 shows the cathode tip and keeper face temperatures versus emission current for the 40 cm engine discharge cathode assembly. Assuming the planar anode discharge approximates the ion engine discharge, the cathode tip temperature, in deg C, can be estimated from:

$$T_{\text{tip}} = 171 \cdot \ln(I_e) + 506 \quad [14]$$

The cathode tip temperature ranged from about 860 degrees C at 7.5 A, to about 1110 degrees C at 35 A. The corresponding keeper face temperature varies from about 405 degrees C to 560 degrees C. The cathode emission currents for the engine during performance testing varied from about 9.4 A at 1.5 kW to 30 A at 7.3 kW. The cathode emission at 10 kW (5.80 A beam current) is estimated to be about 35 A.

The internal pressure of the cathode was also measured. The cathode internal pressure is a strong function of both propellant flow rate and emission currents. At about 15 A emission, the internal pressure varies from about 960 Pascals (7.2 Torr) at 0.30 mg/sec xenon flow rate, up to about 1690 Pascals (12.7 Torr) at 0.88 mg/sec. At 35 A, the pressure varies from 1570 Pascals (11.8 Torr) at 0.59 mg/sec to 1995 Pascals (15.0 Torr) at 0.88 mg/sec.

#### *Ion Optics*

Because 40 cm ion optics were not available for these initial tests, 50 cm ion optics were used. Some differences exist between the 50 cm ion optics used for these tests, and those under fabrication for the 40 cm engine. The accelerator grid electrode for the 50 cm diameter ion optics is about 25% thinner than the NSTAR ion optics and the set of 40 cm optics already manufactured. Additionally, because of some non-uniformity in dish depth between the two 50 cm electrodes, the interelectrode gap was set to about 0.81 mm, instead of 0.66 mm. Also, the 40 cm engine neutralizer had yet not been completed for these tests, so an EM NSTAR neutralizer was used.

Impingement-limited total voltages were measured at beam currents of 1.20, 2.70, 3.52, and 4.75 A. The 40 cm thruster with the 50 cm ion optics was able to successfully operate at the lowest predicted total voltages for all beam currents tested. Impingement-limited total voltages corrected for their larger cold grid gap were less than 50 V higher than those of the NSTAR thruster ion optics.

Radial beam current density profiles at beam currents of 1.20, 2.70, 3.52, and 4.75 A were also documented. Although the beam current density profiles exhibited a repeatable, slightly irregular profile within a 150 mm

radius, there was no substantial peak in the profile center as observed with the DS1 30 cm ion thruster.

### Engine

Preliminary 40 cm engine performance data are listed in Table IV, for power levels ranging from about 1.1-to-7.3 kW. These data are also plotted in Figure 13, engine efficiency versus input power. As indicated, the efficiency at 7.3 kW was approximately 0.68 at 3615 seconds specific impulse, and drops to about 0.51 at 1.1 kW at 2260 seconds specific impulse.

The engine efficiencies documented to date are generally one-to-four percentage points below the goals documented in Table I (for a given propellant throughput and beam voltage). This is due to a combination of factors. The primary factor is the lower performance of the EM NSTAR neutralizer assembly (higher keeper current and propellant flow rate) as compared to that estimated for the 40 cm engine neutralizer still under development. Also a lower discharge propellant efficiency at the lowest throughput condition than anticipated, and a higher accelerator grid drain power at high power (principally a facility effect) contribute to the lower efficiencies. Incorporation of the 40 cm engine neutralizer, 40 cm ion optics, and modification to the discharge chamber are expected to improve the engine performance.

Table IV – Engine Performance

$\dot{m}_T$ , mg/sec	F, mN	$I_{sp}$ , sec	$P_{in}$ , kW	Eff.
2.16	76	1570 V $V_{bps}$ 3560	2.13	0.62
7.89	280	1400 V $V_{bps}$ 3615	7.34	0.68
4.52	160	3605	4.18	0.68
2.16	71	3360	1.93	0.61
4.52	147	1180 V $V_{bps}$ 3310	3.60	0.66
2.16	65	3085	1.67	0.59
4.52	136	1020 V $V_{bps}$ 3070	3.18	0.65
2.10	61	2955	1.48	0.60
2.18	49	680 V $V_{bps}$ 2260	1.09	0.51

### Development Status

Fabrication of two prototype 40 cm engines has been completed, and detailed performance characterizations of both designs are on-going at NASA GRC. Engineering model engine designs, based on the two prototype concepts, have been completed and manufacturing and assembly of the EM engines is nearing completion. Figure 14 is a side-by-side comparison of the DS1 thruster and 40 cm engine.

### Power Processing

A 5 kW breadboard power processing unit (PPU) is being designed and built by Boeing Electron Dynamics Devices under contract with NASA GRC.<sup>5</sup> The 5-kW PPU effort consists of three phases. Phase I includes the overall conceptual design of the PPU and fabrication of the breadboard beam supply. Phase II consists of fabrication of a complete breadboard PPU including integration with a laboratory model 40-cm ion engine. Phase III involves design and fabrication of an engineering model PPU and integration with an engineering model thruster.

The PPU was designed to yield a total efficiency in excess of 92 percent and a total flight-packaged mass of less than 15 kg. This represents a specific mass of 3.0 kg/kW that is half the value for the NSTAR PPU but maintaining the same efficiency. The PPU draws main power from an 80 to 160 V high voltage bus and housekeeping power from a 22 to 34 V low voltage bus. The beam and accelerator supplies have a regulated voltage output and the discharge, neutralizer keeper, and two heaters have a regulated current output. Input/output regulation and output ripple of 5 percent or better is also required. The discharge and neutralizer supplies must include a high voltage pulsed igniter to assist ignition when the hollow cathodes do not breakdown on the power supply open circuit voltage. All the power supplies must be capable of operating under short circuit conditions. Also, the PPU must be capable of operating in a temperature range of -15 to 50 °C, passing MIL-STD-461 for electromagnetic interference (EMI), and exchanging parts with radiation-hardened equivalents.

The beam supply design is critical to obtain high efficiency and low mass since most of the power is

processed by this unit. A modular approach was chosen for this design consisting of four 1.1 kW modules operating in parallel to supply power to the thruster. Further increases in power or N+1 redundancy could be implemented by paralleling additional modules. The topology selected for the beam supply is a phase-shift/pulse-width modulated dual-bridge operating at a switching frequency of 50 kHz. This topology consists of two full bridge power stages operating in parallel on the primary side and in either parallel and/or series on the secondary side. This is attained by a six-diode arrangement and the amount of phase-shift between the two bridges.

Beam power supply efficiencies ranging between 94 to 96 percent were measured for an input voltage range of 80 to 160 V and an output voltage range of 800 to 1500 V for powers from 260 to 1100 W. The total PPU efficiency projections were done using the measured beam supply efficiency numbers and estimated efficiency for the discharge, neutralizer keeper, and accelerator supplies based on the NSTAR PPU performance measurements. The total efficiency for a 5 kW PPU is expected to range from 92 to 95 percent for an output power ranging from 1 to 5 kW. This represents a 1 to 2 percent improvement over the state-of-the-art NSTAR technology.<sup>5</sup>

### Concluding Remarks

The NASA GRC ion propulsion program addresses the need for high specific impulse ion propulsion systems and technology across a broad range of mission applications and power levels. A focussed activity is the development of the next-generation ion propulsion system as follow-on to the Deep-Space 1 system. The system is envisioned to incorporate a lightweight ion engine capable of operating over a 1-10 kW power throttling range with a 550 kg propellant throughput capacity.

An NSTAR-derivative, high-power 40 cm engine is under development. Two engine concepts have been developed to prototype level, and are undergoing detailed performance characterizations. Preliminary performance data for one prototype 40 cm engine has been documented for input power levels ranging from about 1.1 kW to 7.3 kW. The efficiency at 7.3 kW was

approximately 0.68 at 3615 seconds specific impulse. Incorporation of a new neutralizer, ion optics, and modification to the discharge chamber are expected to improve the engine performance by about one to four percentage points across the throttling range. Discharge cathode and magnet temperatures for the 40 cm engine are within design limits and indicate significant margin at full power operation. Engineering model engines and a breadboard power processor are under design and fabrication and will be used as the basis for further advanced hardware development activities.

### References

- [1] Polk, J.E., et al., "Validation of the NSTAR Ion Propulsion System On the Deep Space One Mission: Overview and Initial Results," AIAA Paper No. 99-2274, June 1999.
- [2] Gershman, R., Manager, Planetary Advanced Missions, Jet Propulsion Laboratory, "ESS Technology Requirements," dated June 18, 1999.
- [3] Anon., Integrated In-Space Transportation Planning, Summary of Process and Technology Prioritization, NASA Marshall Space Flight Center, May 2001.
- [4] Personal communication, Anderson, J., Jet Propulsion Laboratory, Pasadena, California, August 2001.
- [5] Pinero, L.R., et al., "Design of a Modular 5-kW Power Processing Unit for the Next-Generation 40-cm Ion Engine," Paper No. IEPC-01-329. Proposed for presentation at the International Electric Propulsion Conference, October, 2001.
- [6] Soulas, G.C., Foster, J.E., and Patterson, M.J., "Performance of Titanium Optics on a NASA 30 cm Ion Thruster," AIAA Paper No. 2000-3814, July 2000.
- [7] Rawlin, V. K., et al., "NSTAR Flight Thruster Qualification Testing," AIAA Paper No. 98-3936, July 1998.
- [8] Wilhelm, H.E., "Quantum Statistical Analysis of Surface Sputtering," *Journal of Spacecraft and Rockets*, Vol. 13, No. 2, February 1976, pp. 116-118.
- [9] Patterson, M.J., et al., "Recent Development Activities in Hollow Cathode Technology," Paper No. IEPC-01-270. Proposed for presentation at the International Electric Propulsion Conference, October 2001.
- [10] Patterson, M.J., "Low-Isp Derated Ion Thruster Operation," AIAA Paper No. 92-3203, July 1992.

[11] Sovey, J.S., "Improved Ion Containment Using a Ring-Cusp Ion Thruster," *Journal of Spacecraft and Rockets*, Vol. 21, Sept.-Oct. 1984, pp. 488-495.

[12] Soulas, G.C., "Design and Performance of 40 cm Ion Optics," proposed for presentation at the International Electric Propulsion Conference, October 2001.

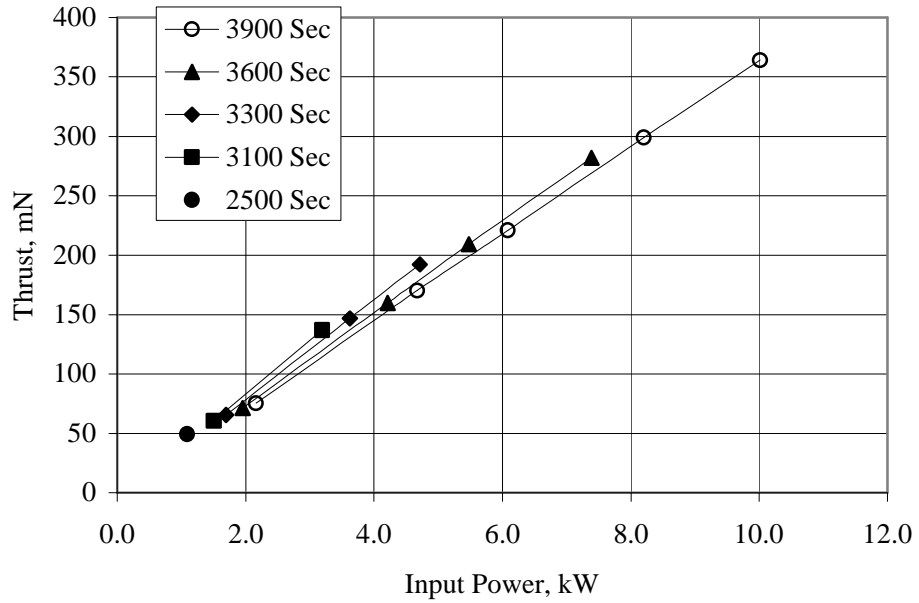


Figure 1 - Estimated thrust and power throttling range for different values of specific impulse.

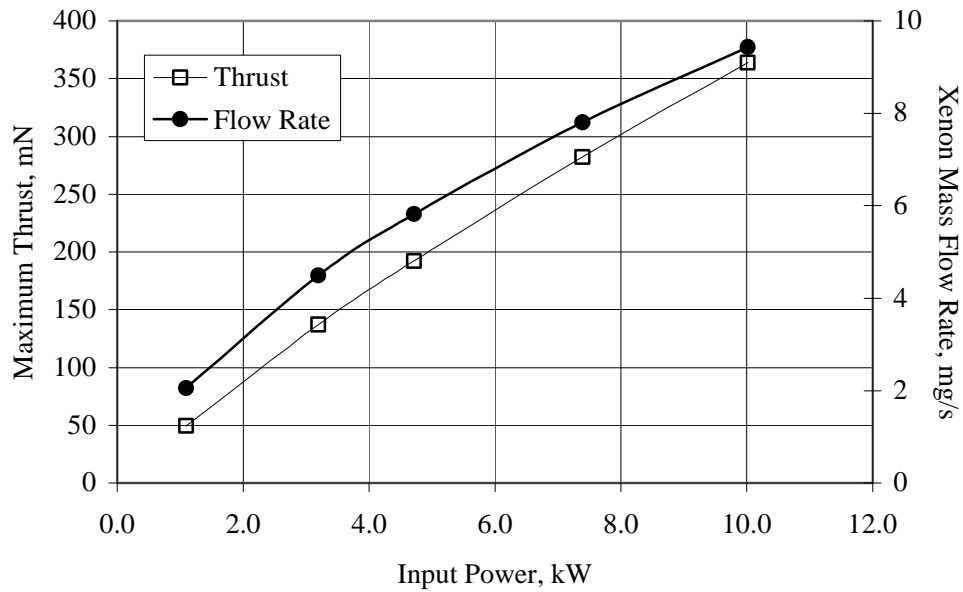


Figure 2 - Estimated thrust and flow rate versus input power to the engine.

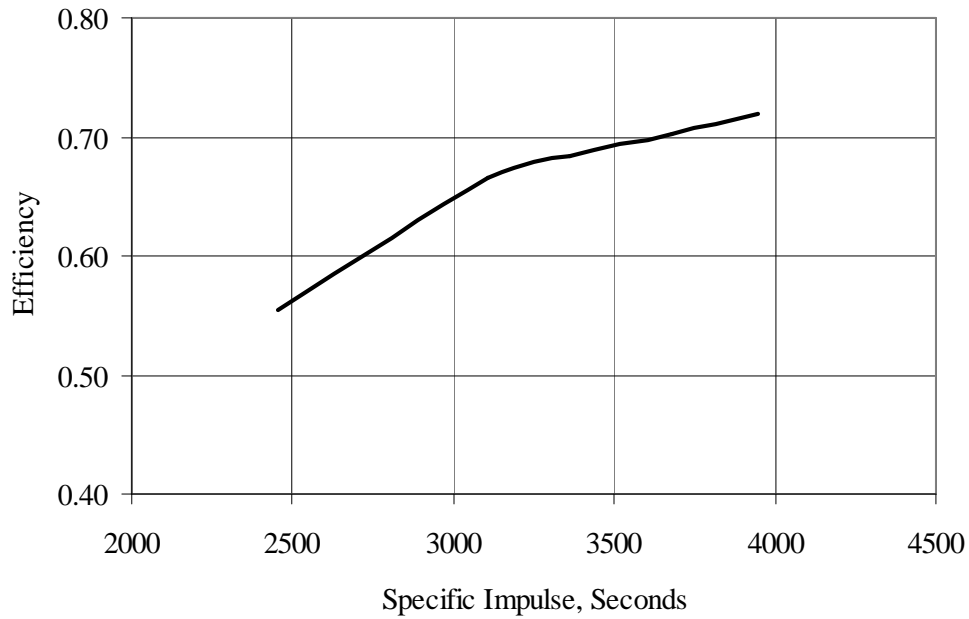


Figure 3 - Estimated thruster efficiency versus specific impulse at maximum thrust.

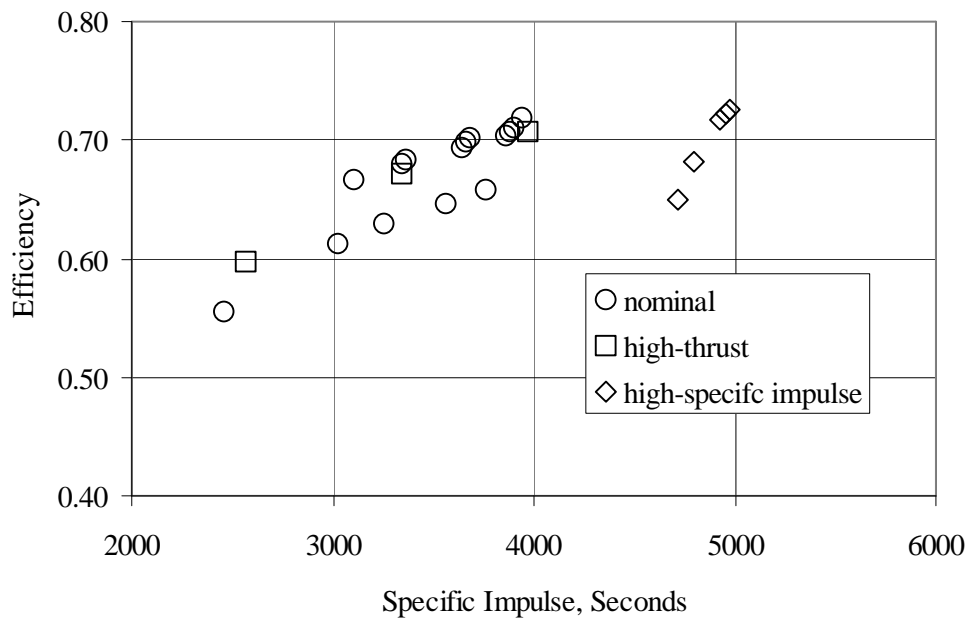


Figure 4. - Thruster efficiency versus specific impulse for various throttling strategies.

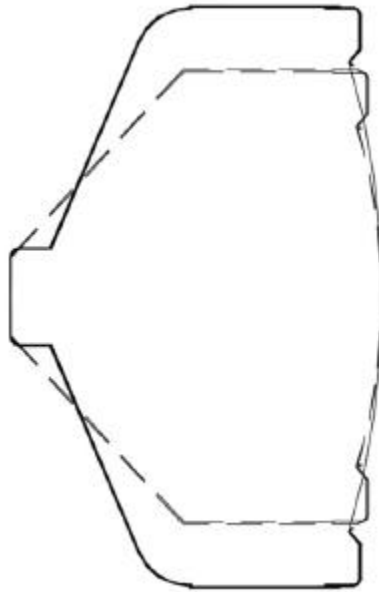


Figure 5 - Superposition of 40 cm engine (solid line) and DS-1 thruster (dashed line) outer mechanical envelope.



Figure 6 - EM engine discharge chambers.

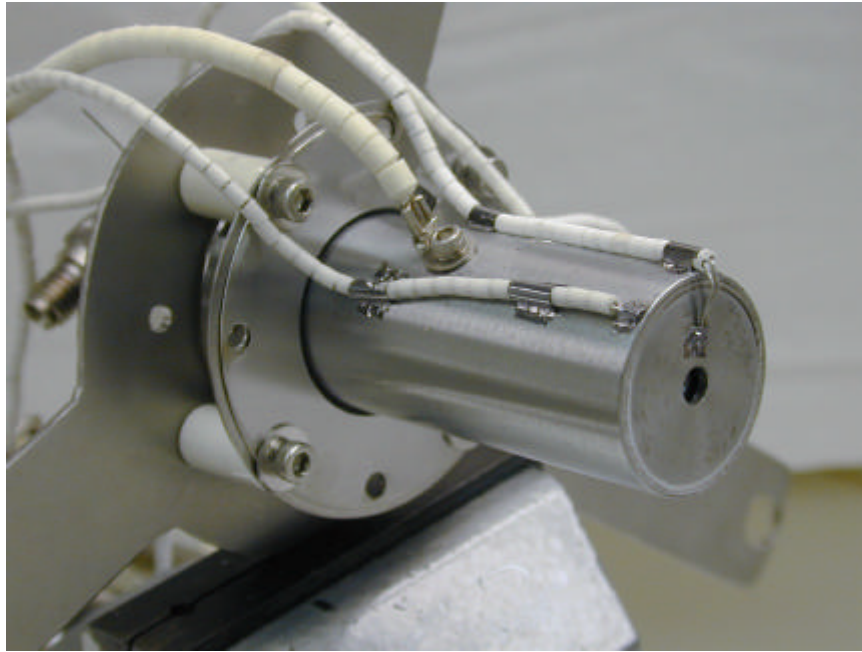


Figure 7 - Prototype discharge cathode assembly for 40 cm engine.



Figure 8 - Photograph of 40 cm screen grid (left foreground) and 40 cm accelerator grid (right foreground) with a 30 cm accelerator grid (center background) for comparison.

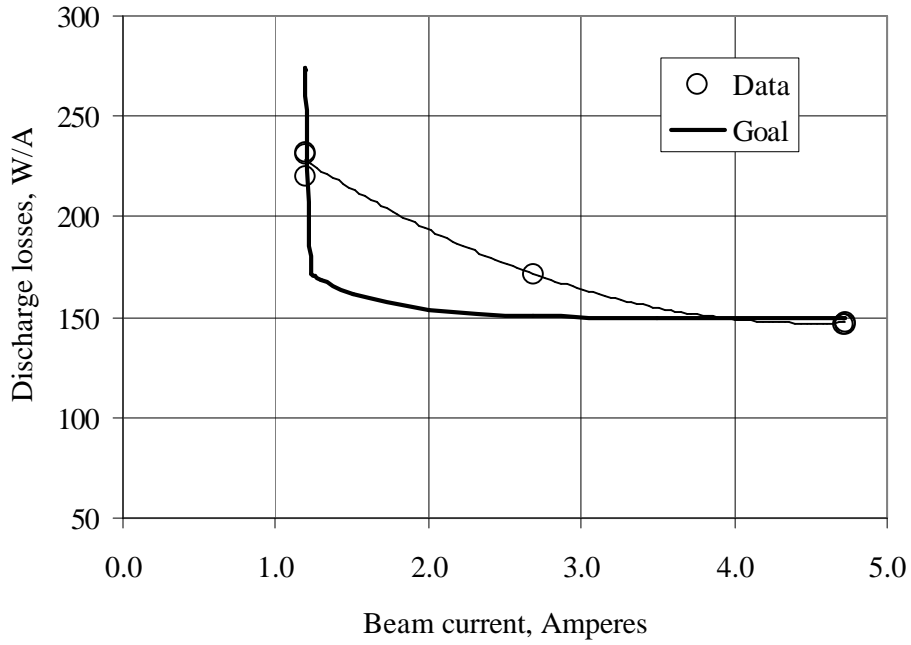


Figure 9 - Discharge losses versus beam current.

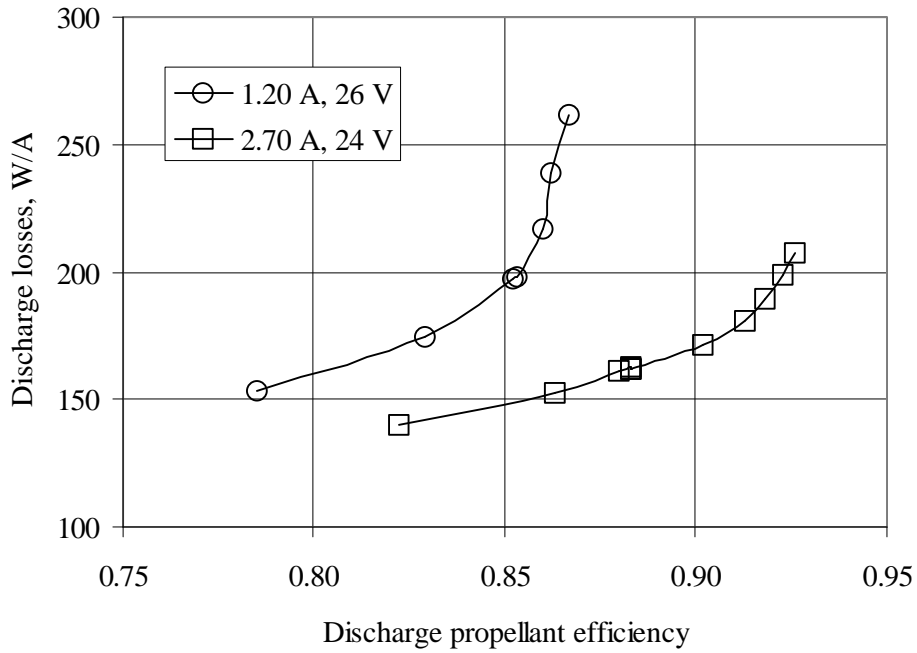


Figure 10 - Discharge losses versus discharge propellant efficiency.

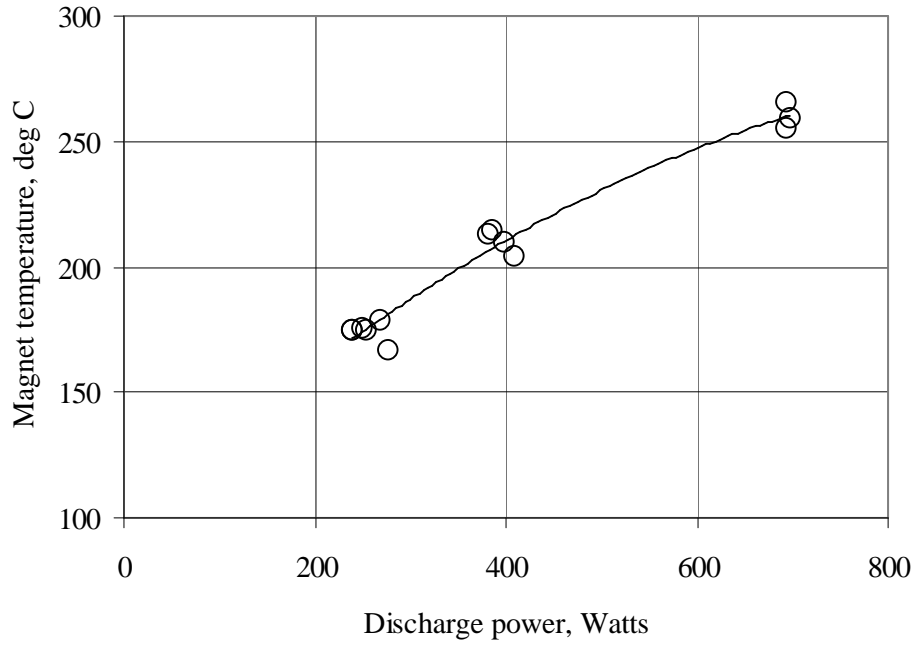


Figure 11 - Magnet temperature versus discharge power.

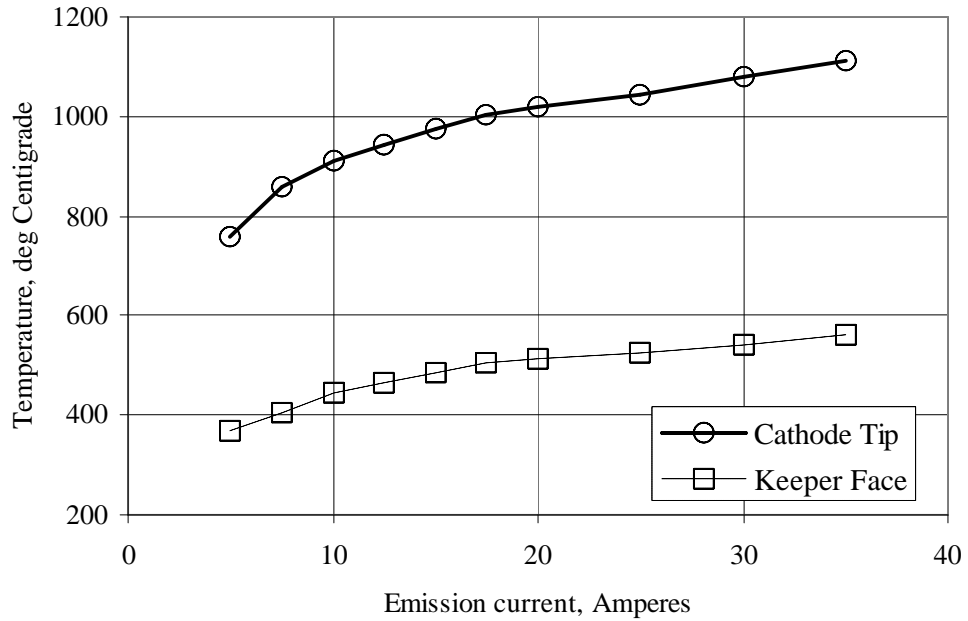


Figure 12 - Cathode temperatures versus emission current; 40 cm thruster discharge cathode.

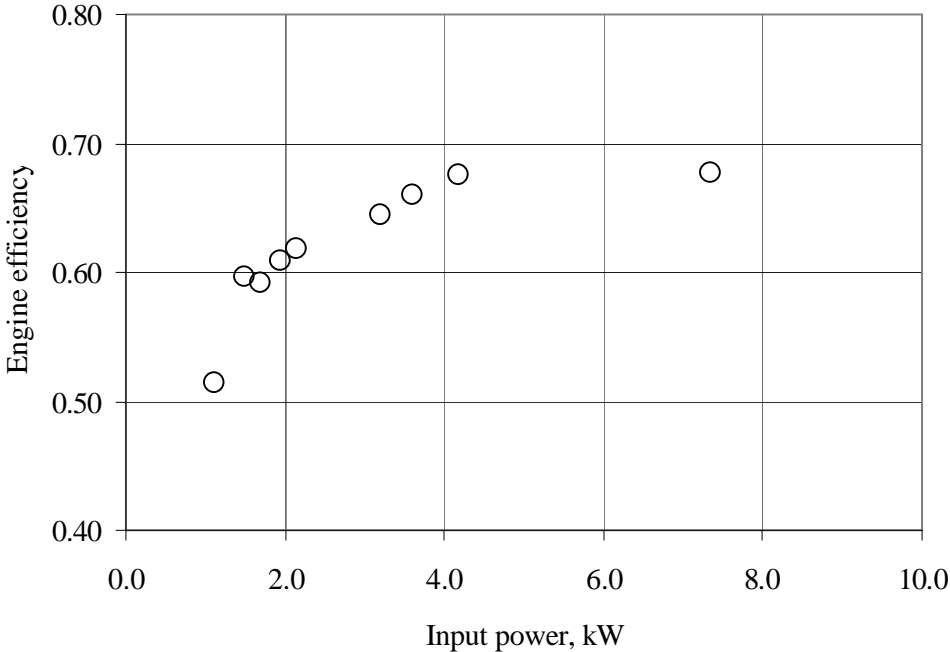


Figure 13 -Engine efficiency versus input power.



Figure 14 - DS1 thruster and 40 cm engine.